Nuclear Mathematical and Computational Sciences: A Century in Review, A Century Anew
Gatlinburg, Tennessee, April 6-11, 2003, on CD-ROM, American Nuclear Society, LaGrange Park, IL (2003)

PEACH BOTTOM BWR TURBINE TRIP BENCHMARK PHASE 3: ANALYSIS OF FULL PLANT SYSTEM WITH 3D-NEUTRONICS USING RETRAN-3D

W. Barten and P. Coddington
Paul Scherrer Institut
CH-5232 Villigen PSI, Switzerland
werner.barten@psi.ch; paul.coddington@psi.ch

ABSTRACT

This paper presents the results of the calculation of the base case of phase 3 of the Peach Bottom Unit 2 Turbine Trip Test 2, OECD/NEA BWR benchmark for coupled thermal-hydraulics and neutronics codes. The plant system transient with the coupling of the full reactor system with 3D-neutronics is calculated using the RETRAN-3D code. The neutronic properties of all 764 fuel assemblies are modeled, each with 24 axial levels. The flow through different sets of fuel assemblies is lumped into 34 thermal-hydraulic channels again with 24 axial nodes. The PSI-RETRAN-3D model gives good agreement with the measured data. The coupling of the effects of the pressure and flow rate oscillations in the steam line, the mass balance in the core, the (void) reactivity and the core power are discussed. The reactivity effects of the change in the core void can explain the overall behavior of the transient for early times and those of the control rods do so for later times. The Doppler reactivity contributes in the second order to terminate the power increase. The time-dependent normalized power of different thermal-hydraulic channels in the core is presented. Up to the time of reactor scram the course of the power is similar for all the channels with differences of the order of a few percent. The axial shape of the channel powers at the time of the maximum power are increased in the core center with respect to the shapes at time zero, by an amount which is different for the different channels.

Key Words: BWR turbine trip, Peach Bottom, coupled codes, systems behavior, 3D-neutronics

1. INTRODUCTION

The Peach Bottom Unit 2 Turbine Trip Test 2 (PB2 TT2) was selected by OECD/NEA as a BWR benchmark for coupled thermal hydraulics and neutronics codes [1]. This benchmark is being performed in three parts (phase 1, 2 and 3), and in addition 3 extreme cases are considered. Benchmarks of this form are very helpful in assessing the capability of codes to analyze complex transients with coupled core-system interactions. Our results of phase 1 using the RETRAN-3D code have been presented in Ref. [2] and the documentation of the phase 2 results are in preparation. This paper presents the results of phase 3 using the RETRAN-3D code [3] to simulate the plant system fully coupled to the core 3D-neutronics and power calculation.

The structure of the paper is as follows. The RETRAN-3D model of the plant and the nodalization used are described in section 2. Our calculations are compared to measured data of the core power and local pressures in section 3. In section 4 the interaction of the flow in the steam line, with the flow balance of the core and the core power are discussed. The 3-

dimensional power distribution is presented in section 5, together with a discussion of the relative changes in the power during the transient. Section 6 gives conclusions.

2. THE RETRAN-3D MODEL

The RETRAN-3D input model for phase 3 is based on the model for the phase 1 calculation [2], which in turn was developed from a RETRAN-02 model [4] for turbine trip 1 and from the benchmark specification contained in Ref. [1]. In the phase 1 calculation the core was represented by a single thermal-hydraulic channel with 24 axial control volumes and the reactor power was taken from the experimental data, while in the current (phase 3) analysis a 3D core is used.

In order to determine the dynamical response of the reactor system it is important to understand the general flow of water in the reactor vessel and how this is approximated using the RETRAN-3D nodalization (Figure 1). Water is pumped from the jet pumps into the lower plenum. From there the flow is upwards into the core region where the water is heated and steam produced. From the core region the steam/water mixture flows into the upper plenum and through the standpipes into the steam/water separator. From the steam/water separator volume the liquid part of the mixture flows into the "steam separator external" volume, while the steam flows through the lower dryer into the steam dome. From there the steam continues into the steam line and the turbine.

From the "steam separator external" volume the liquid flows down into the upper downcomer, while a small amount of steam flows up into the lower dryer volume. From the upper downcomer where the liquid from the "steam separator external" volume is mixed with the feedwater, single-phase (subcooled) water flows down and into the jet pumps.

In order to simulate (within the context of the RETRAN-3D code) the establishment of a liquid level in the "steam separator external" volume and the separation of the steam from the liquid in the steam/water separator volume, the RETRAN-3D bubble rise and two-region non-equilibrium models were used.

Let us now discuss the flow in the core region between the lower plenum and the upper plenum. As documented in the benchmark definition [1], flow from the lower plenum is mainly to the core inlet volume, with a small fraction of the total core flow flowing through the core bypass volume (Figure 2). From the core inlet volume most of the flow continues to the core, while again a small amount enters the core bypass volume. Flow through the core is represented by 34 thermal-hydraulic channels each consisting of 24 axial nodes. Each channel corresponds to the combined flow through a different number of fuel assemblies. The steam/water mixture flowing out of the top of the core channels flows into a single core exit volume and from there flows into the upper plenum where it is mixed with the core bypass flow.

The Zolotar-Lellouche correlation was used to calculate the slip ratio for the two-phase flow, and although the Chexal-Lellouche correlation is the preferred RETRAN-3D slip correlation, it is often difficult to obtain convergence for plant applications, while for the pressures considered

here (>6.0 MPa) the Zolotar-Lellouche slip correlation is shown [5] to give equally good agreement with steady-state void fraction experimental measurements.

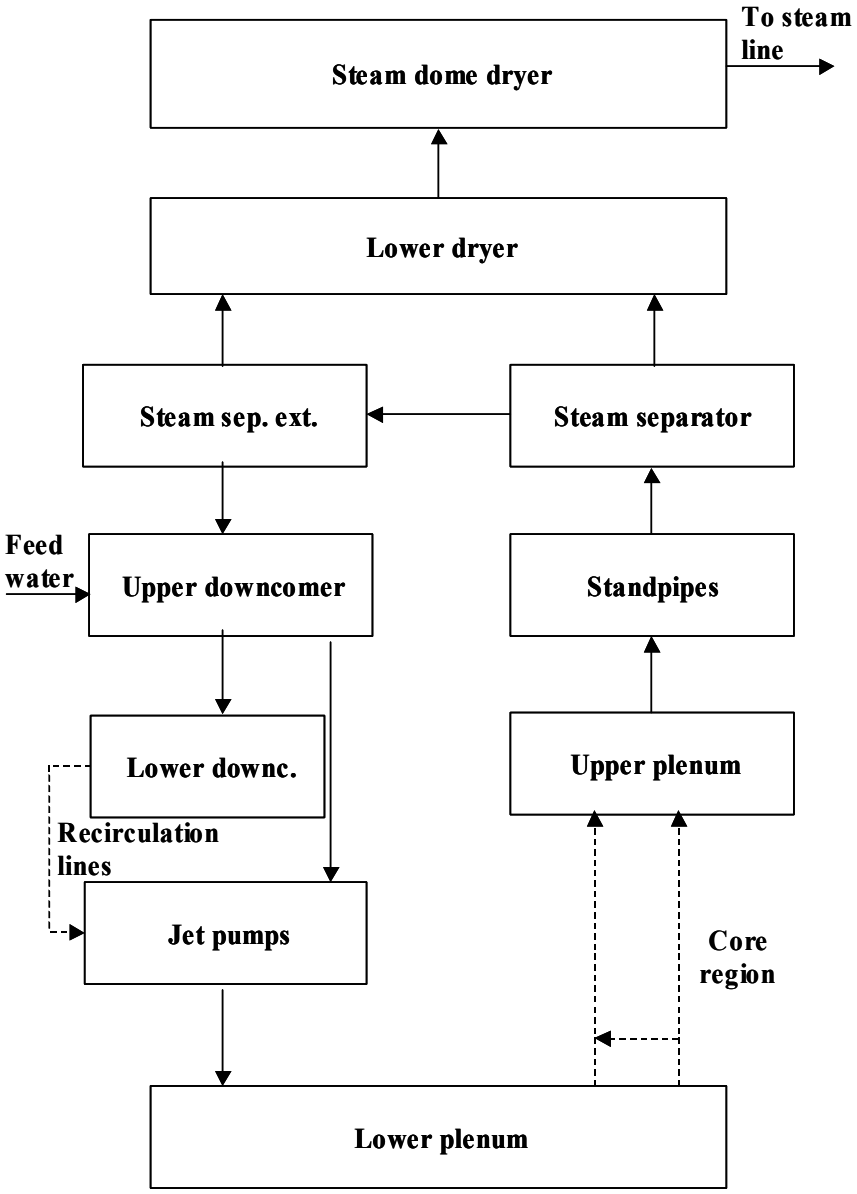

Figure 1. Reactor nodalisation. Not to scale.

For the benchmark phase 3 calculation of the core behaviour presented here, we used a 3D representation of the core. The neutronic parameters of each of the 764 fuel assemblies are entered at 24 axial levels. The combining or "lumping" of the flow through the different fuel assemblies into the 34 thermal-hydraulic channels is that one suggested in Ref. [1, see Fig. 3.2.2] besides that for numerical reasons channel 26 is subdivided here into two different channels, with numbers 26 and 34, see section 5 for more information.

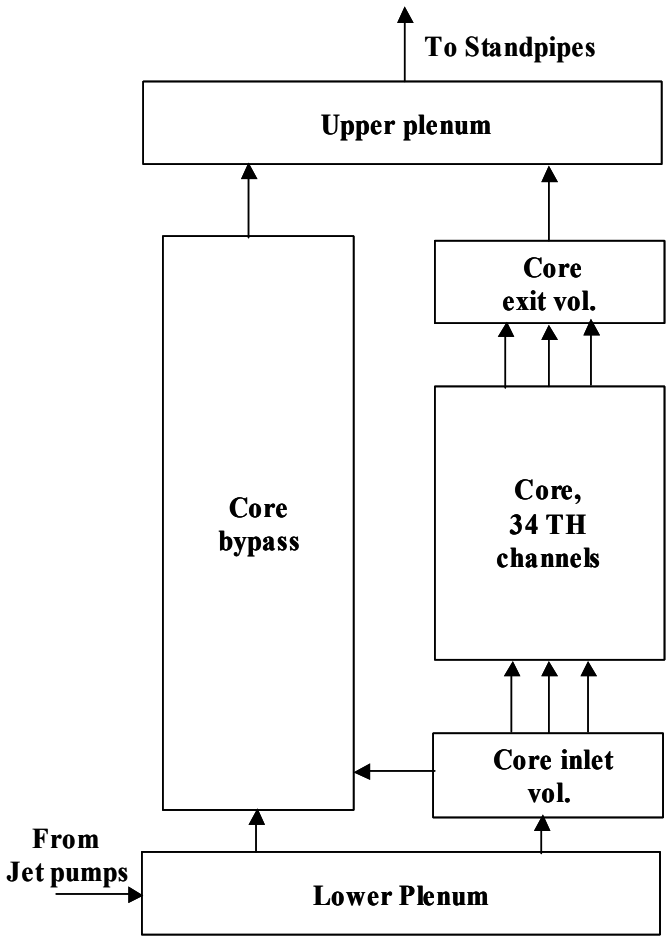

Figure 2. Core region nodalisation. Not to scale.

3. COMPARISON WITH MEASUREMENTS

In this section we compare our RETRAN-3D calculation with measurements obtained from the plant during the transient. Our calculation (Figure 3, black solid lines) is in general in good agreement with the measured data (Figure 3, red dotted lines). The calculated maximum of the normalized power $\overline{Q}(t)$ is only slightly earlier and slightly smaller than the measured value (Figure 3a). The power is normalized to that at time zero.

The thermal-hydraulic behaviour of the reactor as represented by the steam dome (Figure 3b) and the core exit relative pressures (Figure 3c) are well predicted by our RETRAN-3D model. The calculation shows between t = 0.5 sec and 0.9 sec, the initial increase in the pressure as the pressure wave propagates along the steam line from the turbine, followed by the pressure rise as the power increases. The calculation also shows the pressure oscillations due to the pressure wave propagation back and forth along the steam line, with a periodicity of about 1 sec. The flattening of the pressure curve after about 3 sec and the beginning of the decrease as a consequence of the power reduction is also calculated. After about 1 sec the calculated pressures

are about 0.05 MPa below the measured ones. It should be noted that the pressure calculated in phase 3 with the 3D core (black solid lines) is very close and only slightly below our phase 1 calculation with the pre-defined core power (green dashed lines). In our earlier analysis of the system with pre-defined power [2], we discussed improvements of the model in relation to the original base case, in particular with respect to non-equilibrium effects in the steam separator region and to pressure losses in the steam bypass line. The improvements with respect to non-equilibrium effects [2] were included in the 3D model, since they are effective around and in particular before the time to maximum power but those relating to pressure losses in the bypass line being effective only after $t = 2$ sec were not.

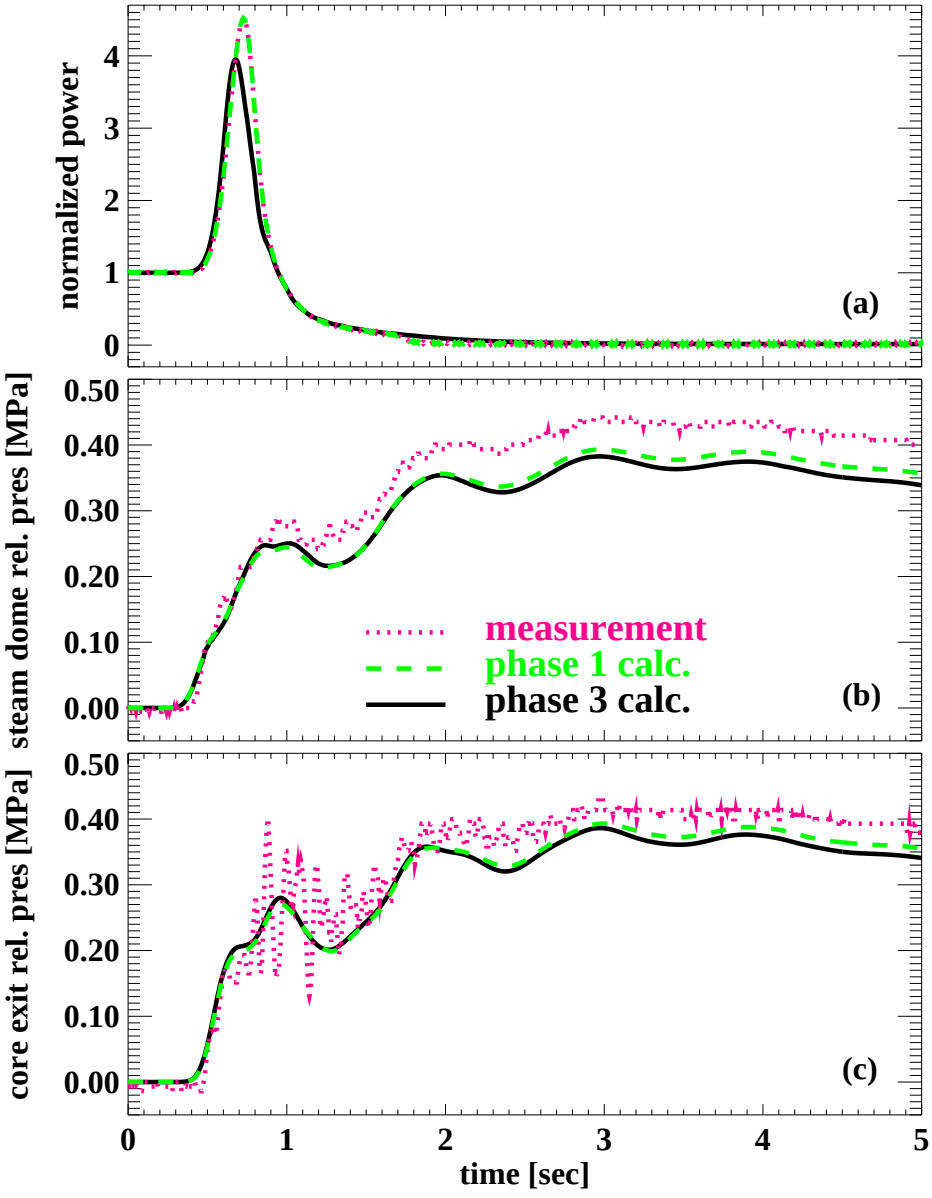

Figure 3. Comparison of calculated and measured power and pressures.

4. DYNAMIC RESPONSE OF THE SYSTEM

In this section we analyze the dynamics of the reactor system during the transient, in particular around the time to maximum power.

4.1. Before Scram

We first discuss the behavior before $t = 0.75$ sec, ie prior to control rod insertion. The transient is initiated at $t = 0$, when the turbine is tripped and the turbine stop valve starts closing. The flow rate from the steam line to the turbine is rapidly reduced from the steady state value of ~1000 kg/sec to zero at $t = 0.096$ sec, when the turbine stop valve is completely closed. Simultaneously at $t = 0.06$ sec the turbine bypass valve begin to open and is full open at 0.852 sec. The flow through the turbine bypass is choked and has a 100% capacity of ~600 kg/sec. The steam line exit flow (Figure 4a, green dashed line) is the sum of the (rapidly decreasing) flow through the turbine and the (slowly increasing) flow through the turbine bypass. It is determined until $t = 0.1$ sec by the flow through the turbine and later by the flow through the turbine bypass. Thus at $t = 0.1$ sec there is nearly no flow at the steam line exit, but at the same time there is still the full flow rate of ~1000 kg/sec at the steam line inlet from the steam dome into the steam line (Figure 4a, black full line). These two effects generate a net mass flow into the steam line. Thus the pressure in the steam line increases, first close to the exit to the turbine. The pressure rise then propagates as a pressure wave back along the steam line to the steam dome leading to a reduction of the steam flow at the steam line inlet with a transit time of ~0.25 sec. After $t = 0.3$ sec the flow at the steam line inlet decreases and falls below zero. Between $t = 0.4$ sec and 0.65 sec there is a reverse flow of steam from the steam line into the steam dome (Figure 4a, black full line), with maximum at $t = 0.46$ sec of -600 kg/sec.

The reduced mass flow after $t = 0.3$ sec between the steam dome and the steam line generates a pressure rise in the steam dome (Figure 3b). This pressure rise then propagates through the steam separator external volume to the lower plenum (Figure 1). The pressure rise at the core inlet (Figure 2) then leads to an increase in the mass flow into the core (Figure 4b, black solid line) with a maximum at $t = 0.5$ sec. In addition the pressure rise in the steam dome propagates down through the steam separator to the upper plenum (Figure 1). The pressure rise at the core exit (Figure 2) results in a reduced mass flow from the core exit (Figure 4b, green dashed line) with a minimum flow at about $t = 0.55$ sec. The response of the flow at the core exit is slower than the response at the core inlet, because the pressure rise (wave) propagates faster through the liquid, in the path from the steam separator external to the lower plenum, than through the (more compressible) steam/water mixture in the path from the steam separator to the upper plenum. The increased core inlet flow and the decreased core exit flow together produce a net positive mass flow into the core (Figure 4b, blue dash-dotted line). The maximum of this net mass flow is about 4000 kg/sec at $t = 0.55$ sec, which is more than double the maximum flow rate reduction at the steam line inlet.

The “squeezing” of the core by the pressure wave propagation through the lower plenum and the upper plenum results in both an increase in the liquid (mass) content of the core and an increase in the core pressure. The net mass flow into the core increases the number of H-atoms in the core, which in turn increases the void (or density) reactivity (Figure 4c, green dashed line).

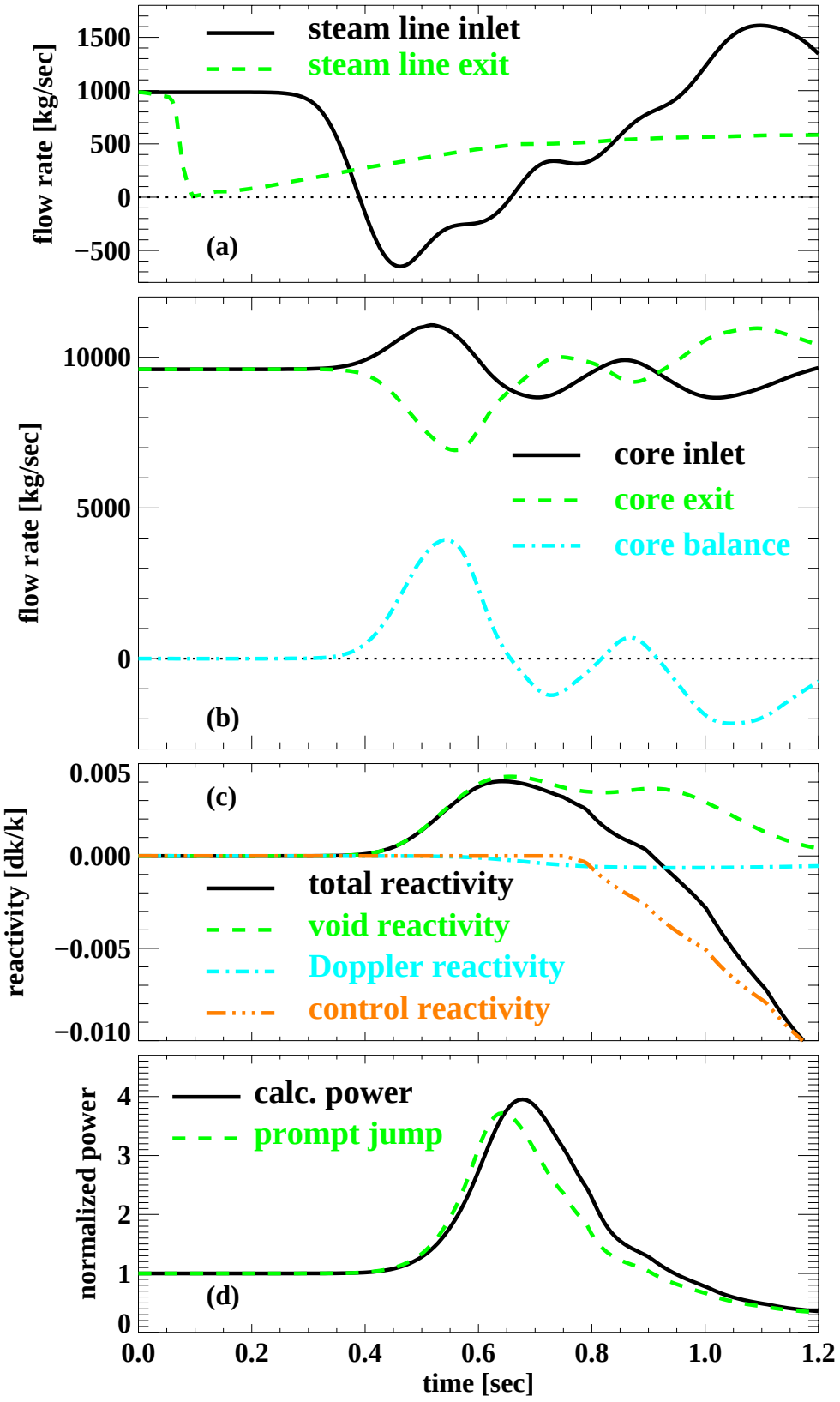

Figure 4. Flow rates, reactivities and power around the time to maximum power.

The increase in reactivity then leads to a power rise (Figure 4d, full black line). The enhanced heat generation and consequently heat transfer to the coolant enhances the vaporization of water in the core, which in turn further increases the core pressure. The core pressure rise balances the pressure at the core inlet and exit, and reverses the mass flow into the core so that after 0.65 sec there is for 0.15 sec a net mass flow out of the core. The result of this is that the void reactivity comes to a maximum at ~ 0.65 s and then slowly decreases. The Doppler reactivity (Figure 4c, blue dash-dotted line) is small and acts only as a second order correction. Thus the total reactivity $\rho(t)$ (Figure 4c, full black line) is dominated by the void reactivity and has its maximum also at about $t = 0.65$ sec. The maximum of the normalized power $\overline{Q}(t)$ follows closely at $t = 0.68$ sec (Figure 4d, full black line). Note that the reduction in the power begins well before the insertion of the control rods at 0.75 sec.

The power behavior can be understood in qualitative terms for this fast transient by a prompt jump approximation [cf. e.g. 6], which predicts the normalized power to be

$$\overline{Q}(t) = \frac{\beta}{\beta - \rho(t)}. \tag{1}$$

The total delayed neutron fraction at the start of the transient is $\beta = 0.005526$ [1, Table 2.3.1]. The power calculated by the prompt jump approximation (Figure 4d, green dashed line) rises slightly earlier than the power calculated by RETRAN-3D, because it assumes an immediate response of the power with respect to the reactivity. The approximated power maximum is slightly earlier than the RETRAN-3D calculation, ie at the time to the reactivity maximum, and it is also smaller, because the increased amount of delayed neutrons due to the power rise is not taken into account in the prompt jump approximation.

4.2. After Scram

The reactor scram is activated at $t = 0.63$ sec, but since the control rods have a response time of 0.12 sec control rod insertion begins at $t = 0.75$ sec. (It should be noted that the scram activation at 0.63s was part of the benchmark specification and is not therefore connected to any plant signal.) The total reactivity is then further reduced by the control reactivity (Figure 4c, brown dash-dot-dot-dotted line). At $t = 0.85$ sec the total reactivity falls below zero. With the further decline of the total reactivity, in particular to negative values the power is more and more reduced. This means that less vapor is produced in the core, which means a net flow into the core.
A continuous net mass flow into the core, however begins only after $t = 1.3$ sec, (ie after the time presented in Figure 4). The mostly negative values of the core flow balance between $t = 0.7$ sec and 1.3 sec are a consequence of the power increase, which leads to an increase in the heat transfer into the coolant and therefore enhanced vaporization and core pressurization. Superimposed on the general behaviour of the core mass balance (Figure 4b) are oscillations, which occur as a consequence of the pressure wave propagation (back and forth) along the steam line.

In addition the oscillations of the steam line inlet flow relative to the steam line exit flow also continue in line with the pressure oscillations in the steam line after the time frame presented in Figure 4, but with decreasing oscillation amplitude.

5. ANALYSIS OF THE THREE-DIMENSIONAL CORE

In the previous section we analyzed the reactivity and total power of the core. In this section we examine the 3-dimensional power shape by analyzing the power in different thermal-hydraulic channels, concentrating on the time before the scram.

5.1. Thermal-hydraulic Channel Radial Map and Control Rod Map

In the present (phase 3) calculation of the core behaviour, we used a 3D representation of the core. The neutronic parameters of each of the 764 fuel assemblies are entered at 24 axial levels. The combining or "lumping" of the flow through the different fuel assemblies into the 34 thermal-hydraulic channels is that one suggested in Ref. [1] besides that for numerical reasons (ie RETRAN-3D will not combine assembly types with different numbers of fuel rods within the same hydraulic channel) channel 26 in [1, Fig. 3.2.2] is subdivided here into two different channels, with numbers 26 (for the 4 more outer fuel assemblies with assembly design 5 [1, Fig. 2.4.2]) and 34 (for the 4 more inner fuel assemblies with assembly design 4). In Figure 5 we show a radial map of the thermal-hydraulic channels where the above-mentioned channels are highlighted. The neutronic parameters of the fuel assemblies and control rods are generated in a manner similar to the PSI RETRAN-3D analysis of phase 2 of the benchmark, which again are generated in the same way as those for the CORETRAN analysis [7] of phase 2 of the benchmark.

The reactor core contained a complex pattern of control rods prior to the initiation of the transient, (Figure 5) with a significant number of partially inserted rods. The details of the control rod pattern are given in [1, Fig. 5.2.1], while some important features of this pattern are the following; a bank of 4 control rods inserted by 1/3, surrounds the inner part of the core, this region is then surrounded by another bank of 8 control rods, which are almost fully (11/12) inserted, outside of this is a ring of 24 control rods, which are inserted 1/4 to ½, and finally on the outside is a ring of 24 control rods consisting of 8 fully inserted control rods, 12 control rods with ~1/4 insertion and 4 control rods with 1/6 insertion.

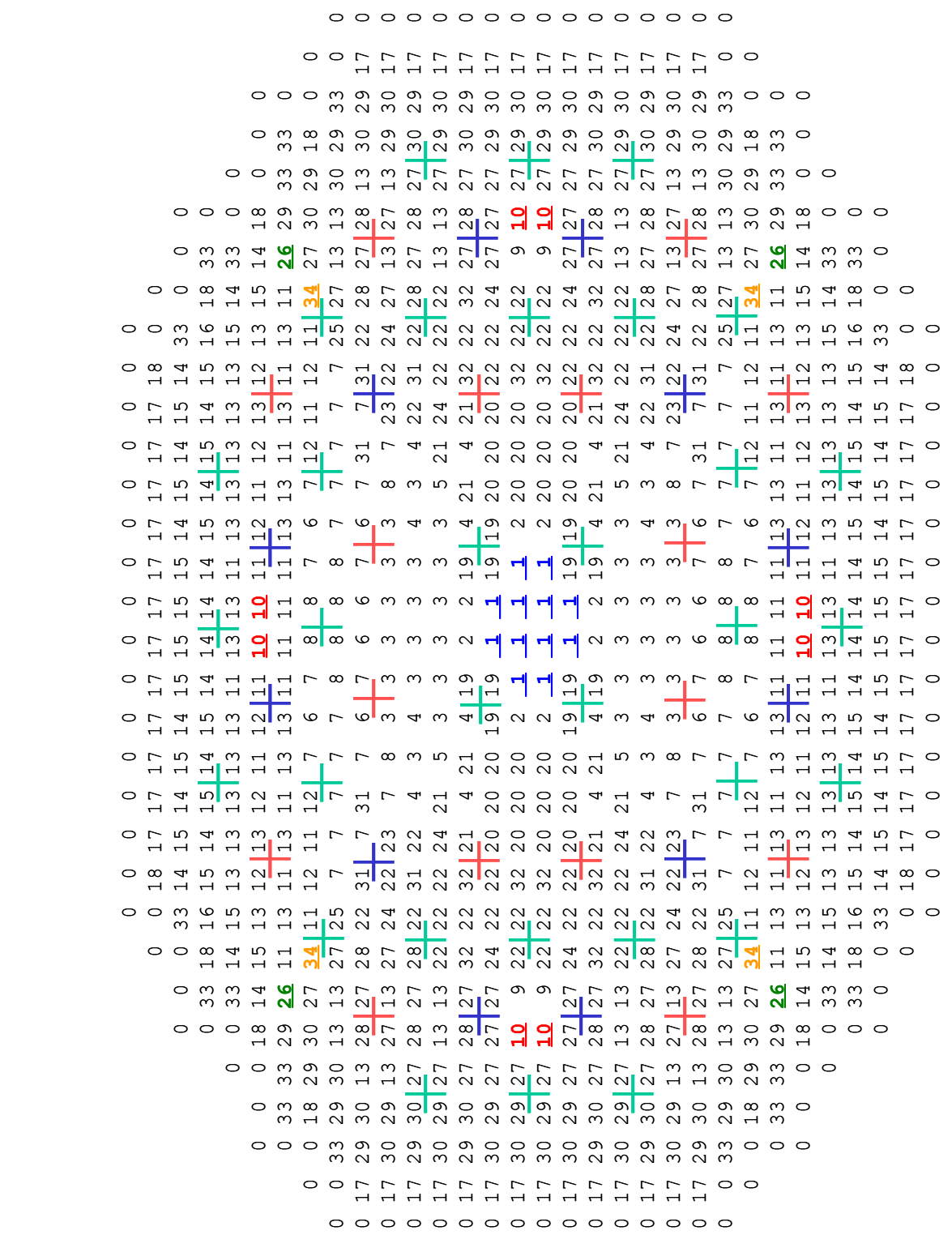

Figure 5. Thermal-hydraulic channel radial map. Channels 1, 10, 26, 34 are highlighted. Control rods are given as + symbols: 1/6 to 1/3 inserted (green), ~1/2 (blue), 11/12 to 1 (red).

5.2. Channel Averaged Power

The change in the power production (as a function of time) in the different fuel assemblies is almost homogenous. To illustrate this we analyze the power produced in different thermal-hydraulic channels. In Figure 6 the normalized power of the fuel assemblies in the channels 1, 10 and 26 (Figure 5) are shown. Channel 1 is representative of the channels inside the ring of 8 nearly fully inserted control rods. Channel 10 is typical of the channels outside this ring and has the highest power at the time of maximum power and the second highest power at time zero. Channel 26 is close to the periphery of the core and is the farthest removed from the region with control rods.

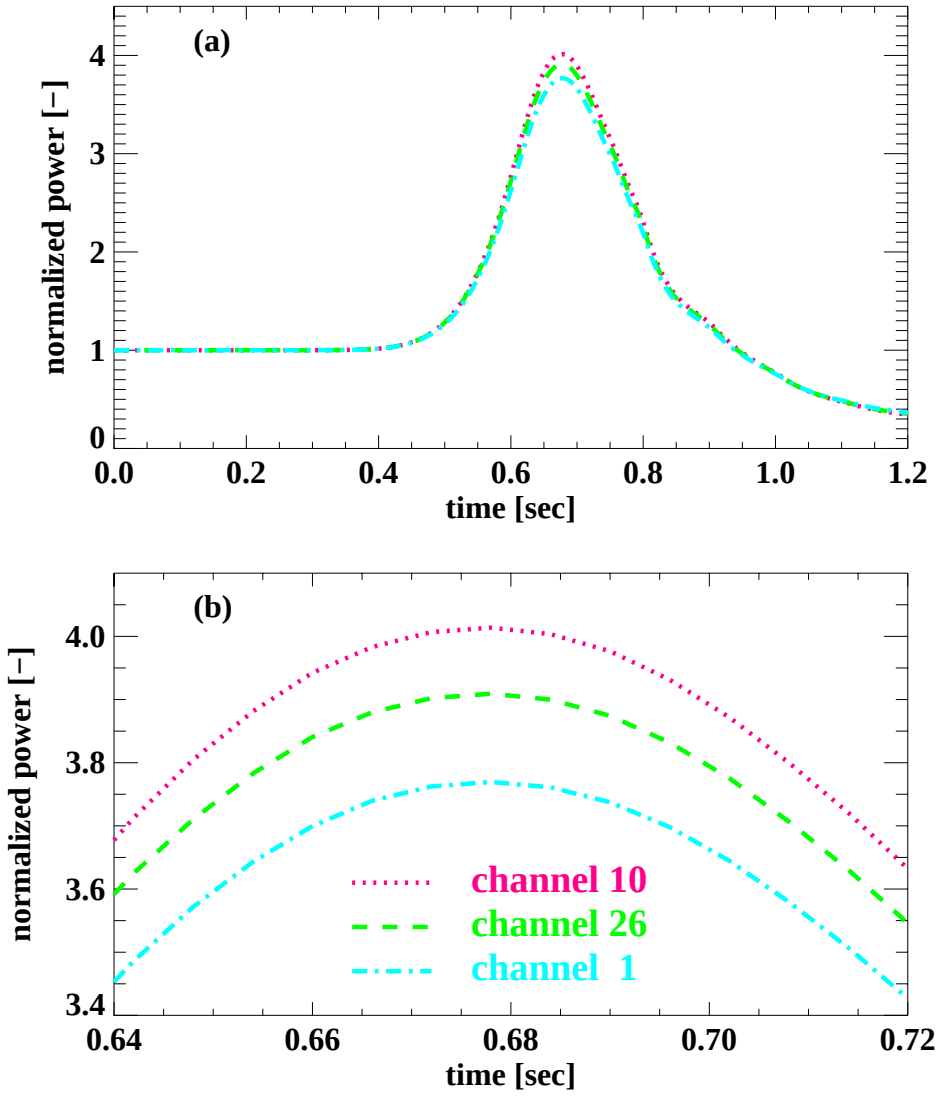

Figure 6. Time-dependent channel power.

Figure 6a shows the power between zero and $t = 1.2$ sec, while Figure 6b gives the detailed behavior around the maximum. The time-dependency of the power in the individual channels is

almost identical. The rise of the normalized power in the maximum power channel (channel 10) (Figure 6b, red dotted line) is slightly larger than that in channel 26 (green dashed line), which again is larger than that in the center of the core ie channel 1 (blue dash-dotted line). The differences are only a few percent.

5.3. Axial Profiles of Channel Power

We continue the analysis of the channel powers by examining their axial profiles. We consider the node wise defined power density where at each time the power density in each channel is normalized to a value of 1.0.

Figure 7a shows the normalized power density $\hat{Q}_{ch,no}(t=0)$ at time zero for channels $ch = 1, 10, 26$ (Figure 5). The axial profiles are different in shape and magnitude. Channels 1 and 10 have their power maximum about at mid-height with an asymmetry around their maximum, such that the power increase below the maximum is steeper than the power decrease above the maximum. This is the typical behaviour for most of the channels in the core. Channel 26 and some channels at the periphery of the core have their power maximum close to the bottom of the core. This is because of the zero void at the core inlet and because channel 26 is far removed from the control rod banks and in particular from those banks with partly inserted control rods. The power in the fuel assemblies in the center of the core, surrounded by the second, nearly fully inserted ring of control rods is of similar shape to channel 1, with a plateau at the lower end of the core. This reflects the influence of the inner most bank of control rods, which is inserted by 1/3 and surrounds the center of the core (Figure 5). Channel 10 shows the typical axial power profile of the channels outside the second ring of control rods. The power in the lower half of the channel is depressed, but there is no singular signature for the location of the tip of an individual control rod. Of course, channel 10 is surrounded by control rods which are inserted by different amounts, ~1/4, 1/3, 1/2.

The overall observation therefore is that because of the complex control rod pattern present in the core prior to the transient initiation there is a large range of different channel/fuel assembly axial power profiles.

At the time of the power maximum the axial shapes of the channel power densities are similar to that at time zero, with some small changes (Figure 7b). On the average, the normalized power density $\hat{Q}_{ch,no}(t_{\max})$ in channel 1 is decreased by about 4% and in channel 26 by about 1.5%, while in channel 10 it is increased by about 1.5%. Channel 10 has the highest axially averaged power density and also the highest node based power density at the time of the power maximum. The relative decrease in the center (channel 1) is due to the higher control rod density.

All channels show a similar behaviour in the axial redistribution of their normalized power densities. For example (for all channels) the relative power density is increased at the mid-height and reduced at the lower and upper ends. This can best be seen in Figure 7c, where the change in the normalized power density, $\hat{Q}_{ch,no}(t_{\max}) - \hat{Q}_{ch,no}(t=0)$, is shown. The power maximum of channel 10 is increased by about 9% and channel 1 by about 3%, while the axial location of the power maximum of channel 26 is moved towards mid-height.

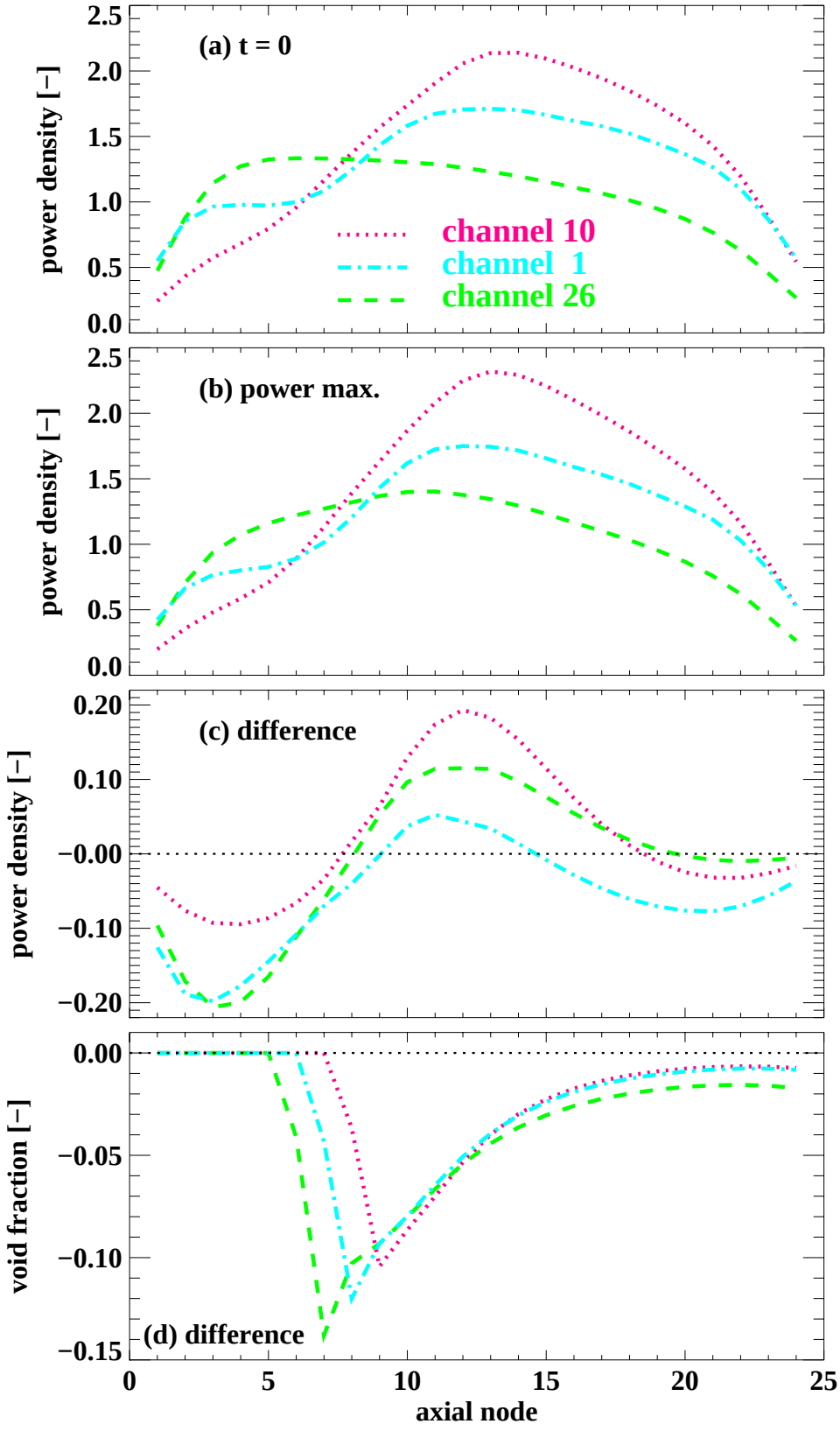

Figure 7. Axial profiles of channel power and void.

As noted before, there was no movement of the control rods before the scram. Thus all these changes and in particular the redistribution in the axial power density profiles are induced by the changes in the void reactivity and the influence of the complex ring pattern of control rods. In fact, the largest change in the local void occurs immediately above the onset of boiling (Figure 7d). This is produced as a result of the combination of the following three effects. First, the increased flow rate of water at the core inlet moves the boiling boundary instantaneously vertically upward, second, the increased pressure in the core leads to a general collapse of the void, while finally, because of the relatively long core transit time (~2 sec) the locally produced void is not connected over the length of the core such that there is not sufficient steam produced over the short time period (only 0.2 to 0.3 sec) to lower the liquid level, as a steady-state investigation (e.g. [8,9]) would suggest.

6. CONCLUSIONS

The results of the RETRAN-3D calculations for phase 3 of the Peach Bottom 2 Turbine Trip 2 benchmark, presented here are in good agreement with the measured data and in particular the power, the steam dome pressure and the core exit pressure. These calculations were performed using RETRAN-3D, with the plant system model coupled to a 3D neutronics solution, where the flow in the core is combined into 34 thermal-hydraulic channels.

The transient with the following sequence of effects is well represented. First, the closure of the turbine stop valve and thereby the stagnation of the steam flow leads a pressure wave in the steam line. The pressure wave is propagated back along the steam line and leads for a short period to a reverse flow of steam from the steam line into the reactor vessel steam dome. The pressure wave then propagates further down into the reactor vessel, leading to an increase in the flow from the lower plenum into the core and a reduction in the flow out of the core into the upper plenum. These two effects combine to produce a net mass flow into the core. The amplitude of the maximum net mass flow into the core is more than double the reduction in the flow into the steam line. The net mass flow into the core increases the void reactivity, which generates a subsequent power excursion. The enhanced heat transfer on the other hand intensifies the boiling in the core, which increases the core pressure and so leads to a mass flow out of the core. This then reduces the void reactivity and consequently also the power. After the power peak the plant is shut down with a scram. Thus the reactivity effects resulting from the change in the core void can explain the overall behavior of the transient for early times ie up to the time of the reactor scram. The Doppler reactivity provides a second order contribution to the termination of the power increase. We have also shown that the coupling of the neutronics to the plant system can also be understood in qualitative terms by a prompt jump approximation for this fast transient.

Finally we have investigated the 3D nature of the core power distribution by analyzing the power density of the different thermal-hydraulic channels. The time dependence of the channel-averaged power is quite similar for the different channels, while the differences in the relative power (between all the channels) at the time of the power maximum are within a few percent. The axial distribution of the channel power at the time of the maximum power with respect to that at time zero shows a relative increase in the power at the core center, but by a different

amount for each channel. The changes in the power shape occur as a consequence of both the change in the void profile in each of the different channels, and the influence on the different fuel assemblies of the complex ring-pattern of the control rods.

ACKNOWLEDGMENTS

The introduction of the neutronic parameters into our RETRAN-3D model by Hakim Ferroukhi is gratefully acknowledged. Thanks to Hakim Ferroukhi and Garry Gose for realization of the effective core bypass density correction in the RETRAN-3D code. This work was partly funded by the Swiss Federal Nuclear Safety Inspectorate HSK (Hauptabteilung für die Sicherheit der Kernanlagen) and the Swiss Federal Office of Energy BFE (Bundesamt für Energie).

REFERENCES

1. J. Solis, K. N. Ivanov, B. Sarikaya, A. M. Olson, and K. W. Hunt, Boiling water reactor turbine trip (TT) benchmark, Volume I: Final Specifications, NEA/NSC/DOC(2001)1 (June 2001).
2. W. Barten, P. Coddington, and H. Ferroukhi, "Peach Bottom BWR Turbine Trip Benchmark: PSI Analysis of Exercise 1 Using RETRAN-3D", *Proceeding of the PHYSOR 2002 Conference*, Seoul, Korea, on CD-ROM, October 7-10 (2002).
3. M. P. Paulsen, C. E. Peterson, G. C. Gose, J. H. McFadden, J. G. Shatford, J. L. Westacott, P. P. Cebull, J. Y. Wu, and P. J. Jensen, RETRAN-3D — A Program for Transient Thermal-Hydraulic Analysis of Complex Fluid Flow Systems, Volume 1: Theory and Numerics, Volume 3: User's Manual, Computer Simulation & Analysis, Inc., Idaho Falls, Idaho, USA (2001).
4. K. Hornyik, and J. A. Naser, RETRAN Analysis of the Turbine Trip Tests at Peach Bottom Atomic Power Station Unit 2 at the End of Cycle 2, EPRI Special Report, NP-1076-SR, EPRI, Palo Alto, California, USA (1979).
5. D. Meier, and P. Coddington, "Evaluation of the Slip Options in RETRAN-3D", *Nuclear Technology*, **128**, pp.153-168 (1999).
6. D. L. Hetrick, *Dynamics of Nuclear Reactors*, The University of Chicago Press, Chicago, USA (1971).
7. H. Ferroukhi, W. Barten, and P. Coddington, "Transient 3-D Neutron Kinetic Analysis with CORETRAN of the Peach Bottom 2 Turbine Trip Benchmark Core Thermal-Hydraulic Boundary Condition Model", *Proceeding of the PHYSOR 2002 Conference*, Seoul, Korea, on CD-ROM, October 7-10 (2002).
8. L. S. Tong, and Y. S. Tang, *Boiling Heat Transfer and Two-Phase Flow*, Taylor and Francis, Washington, D.C., USA (1997).
9. W. Barten, "RETRAN-3D Results and One-dimensional Analytical Model for the Critical Power of a Rod Bundle with Cosine-shape Heating", *Proceeding of the Jahrestagung Kerntechnik 2001, Annual Meeting on Nuclear Technology 2001*, Dresden, Germany, May 15-17, 2001, p. 333-337, INFORUM Verlag, Bonn (2001).